# Time Shift Governor for Spacecraft Proximity Operation in Elliptic Orbits

Taehyeun Kim\*, Ilya Kolmanovsky<sup>†</sup>, and Anouck Girard<sup>‡</sup>
Department of Aerospace Engineering, University of Michigan, Ann Arbor, 48109 MI, USA

This paper presents a parameter governor-based control approach to constrained spacecraft rendezvous and docking (RVD) in the setting of the Two-Body problem with gravitational perturbations. An add-on to the nominal closed-loop system, the Time Shift Governor (TSG) is developed, which provides a time-shifted Chief spacecraft trajectory as a target reference for the Deputy spacecraft, and enforces various constraints during RVD missions, such as Line of Sight cone constraints, total magnitude of thrust limit, relative velocity constraint, and exponential convergence to the target during RVD missions. As the time shift diminishes to zero, the virtual target incrementally aligns with the Chief spacecraft over time. The RVD mission is completed when the Deputy spacecraft achieves the virtual target with zero time shift, which corresponds to the Chief spacecraft. Simulation results for the RVD mission in an elliptic orbit around the Earth are presented to validate the proposed control strategy.

### I. Introduction

Many spacecraft rendezvous and docking (RVD) missions have been planned and successfully performed. Such RVD missions allow exchanging crews or/and cargo in satellites and space stations.

RVD has been an important topic throughout the history of spaceflight. In 1966 the first RVD mission has been manually conducted in a Gemini program. In the following year, the spacecraft Cosmos 186 and 188 have opened a new chapter in the uncrewed RVD missions. Examples of more recent RVD missions are Crew-6 docking at ISS and the planned chaser cargo system to provide delivery services to the space station and return cargo to the Earth [1, 2].

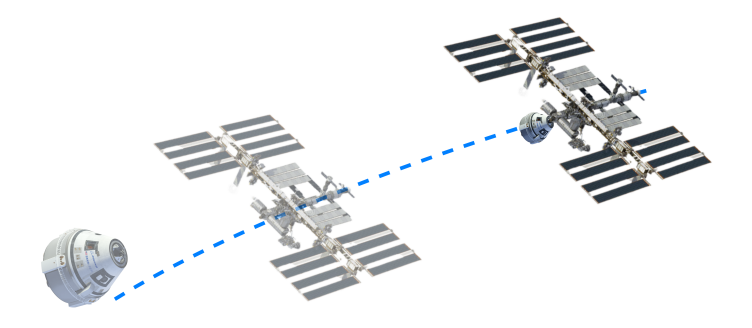


Fig. 1 Spacecraft rendezvous and docking mission on an elliptic orbit.

In this work, we address a spacecraft RVD problem on elliptic orbits. A number of satellites have orbited along elliptic orbits for various purposes, such as Earth observation, communications, and gravity assist for

<sup>\*</sup>Ph.D. student, Aerospace Engineering, 1320 Beal Ave, Ann Arbor, MI 48109

<sup>†</sup>Professor, Aerospace Engineering, 3038 FXB, 1320 Beal Ave, Ann Arbor, MI 48109, AIAA Associate Fellow.

 $<sup>^{\</sup>ddagger}$ Professor, Robotics and Aerospace Engineering, 3264 FMCRB, 2505 Hayward Street, Ann Arbor, MI 48109, AIAA Associate Fellow.

interplanetary missions. For example, the Molniya orbit is a satellite orbit intended to provide communications over high latitudes. After the first successful insertion into this Molniya orbit in 1964, many communication satellites have used this orbit [3]. Tundra orbit has been employed by Sirius satellite radio [4], and has also been studied as a potential disposal orbit [5].

The control systems in RVD missions must strictly adhere to many constraints. In particular, in the docking phase, it is crucial to satisfy the Line-of-Sight (LoS) constraint to guarantee that the docking sensor or fiducial markers are visible [6]. The approach velocity limit is crucial when the spacecraft is in the vicinity of the target object to decrease the risk of damage if there is a high velocity collision. Lastly, the thrusters can only deliver limited thrust.

Many guidance and control methods have been developed for spacecraft proximity operations. In particular, artificial potential function (APF)-based guidance has been implemented for the spacecraft rendezvous and docking problems [7–9]. The APF-based methods can deal with path constraints by defining a potential function that has high values in regions which spacecraft is required to avoid, and low values at the target spacecraft location. The APF-based solution is, however, not optimal, and may not simultaneously handle approach velocity constraints and thrust limits. Model predictive control (MPC) has been studied extensively for spacecraft maneuvers with a variety of constraints [10, 11] and has been successfully used in the PRISMA proximity operation demonstration mission [12, 13]. However, MPC has a high onboard computational cost [14, 15].

# II. Time Shift Governor Approach

In this paper, we develop the Time Shift Governor (TSG) to address the constrained RVD problem between an active chaser and a passive target in an elliptic Earth orbit in the setting of the Two-Body problem, including the  $J_2$  effects. The TSG enforces the constraints by adjusting a single parameter which is the time shift of the target trajectory commanded to the nominal controller. Previously, this approach had been proposed for constrained spacecraft formation control on circular Earth orbits [16, 17] and exploited for spacecraft RVD on Halo orbits in the setting of the Three Body Problem [18]. TSG belongs to a larger set of techniques used to coordinate motions by modifying the allocation of space and time along predetermined paths. For instance, [19] presents a related approach in the context of multirotor unmanned aerial vehicles.

TSG is also a variant of the parameter governor scheme [20], which is an add-on control scheme for adjusting parameters in the nominal closed-loop control system to enforce pointwise-in-time state and control constraints. As compared to more general model predictive controllers, parameter governors can often be implemented at a low computation cost. This efficiency is attained by solving online a low-dimensional optimization problem based only on a small set of parameters that can be assigned discrete values.

# III. Time Shift Governor Development

## A. Problem Formulation

In this work, we consider a spacecraft docking mission in an elliptic orbit around the Earth subject to multiple mission-specific constraints. During the docking mission, the secondary (Deputy) spacecraft is located near the primary (Chief) spacecraft. We use subscripts c and d to denote the Chief spacecraft and the Deputy spacecraft, respectively, and we use the subscript i to denote spacecraft that can either be the Chief or the Deputy.

# 1. Dynamics

The equations of motion of each spacecraft are given by

$$\dot{X}_i = f(t, X_i(t), u_i(t)), \tag{1}$$

where  $X_i = [x_i, y_i, z_i, \dot{x}_i, \dot{y}_i, \dot{z}_i]^\mathsf{T} \in \mathbb{R}^n$  and  $u = [u_1, u_2, u_3]^\mathsf{T} \in \mathbb{R}^p$  stand for the spacecraft state and the control input to the spacecraft, repectively, expressed in the Earth-centered inertial (ECI) coordinate frame. Equation (1) represents the motion for spacecraft translational dynamics, including the perturbation effects and is derived from Newton's second law,

$$\ddot{\vec{r}} = -\frac{\mu}{r^3} \vec{r} + \vec{a}_j + \vec{u},\tag{2}$$

where  $\mu$  and j denote, respectively, the gravitational parameter and the index of perturbation sources,  $\vec{r} = [x, y, z]^T$  is the spacecraft position vector, and r is its 2-norm, e.g.,  $r = ||\vec{r}||$ .

Assuming the primary body is axially symmetric, the gravitational potential, U, is expressed as,

$$U(r,\phi) = -\frac{\mu}{r} \left[ 1 - \sum_{k=2}^{\infty} \left( \frac{r_{eq}}{r} \right)^k J_k P_k(\sin \phi) \right],\tag{3}$$

where  $\phi$  is the latitude of the satellite,  $r_{eq}$  is the equatorial radius of the primary body, and  $J_k$  is the zonal gravitational harmonics constant. We use the second zonal harmonics term ( $J_2$  in our model) to reflect the dominant effects of the Earth's oblateness perturbation [21, 22]. The corresponding  $J_2$  perturbing acceleration is given by

$$\vec{a}_{J_2} = -\vec{\nabla}_{\vec{r}} \left( -\frac{\mu}{r} \left( \frac{r_{eq}}{r} \right)^2 J_2 P_2(\sin \phi) \right) = -\vec{\nabla}_{\vec{r}} \left( \frac{\mu}{r} \left( \frac{r_{eq}}{r} \right)^2 J_2(3\sin^2 \phi - 1) \right). \tag{4}$$

## 2. Coordinate systems

In this paper, we use two coordinate systems: the Earth-centered inertial (ECI) and local Velocity-Normal-Binormal (VNB) frames. The ECI frame, which expresses the dynamics of spacecraft, is defined as  $E : \{O_E, i_E, j_E, k_E\}$  where  $O_E$  is the center of the Earth,  $i_E$  points to the vernal equinox,  $k_E$  is the Earth's rotational axis direction, and  $j_E$  completes a right-handed frame, as shown in Fig. 2.

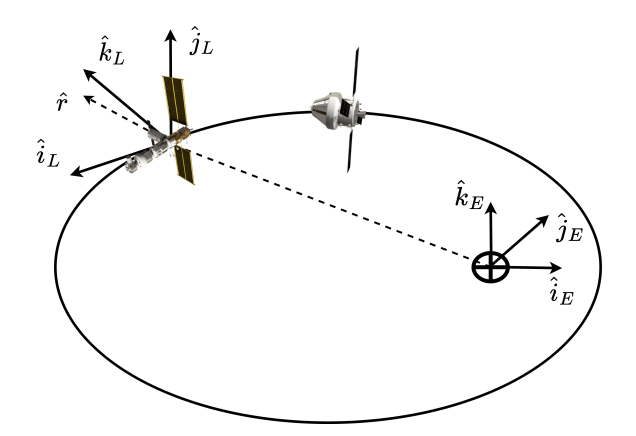


Fig. 2 Earth-centered inertial frame and VNB frame.

To show cone angle constraint in a graphical way, we also defined a local VNB frame as  $L: \{O_c, i_L, j_L, k_L\}$  where  $O_c$  is located at the Chief spacecraft location,  $i_L$  aligns with the Chief velocity vector,  $j_L$  is along the cross product of the Chief position vector relative to the center of the Earth with the Chief velocity vector direction  $i_L$ , e.g., the direction of the orbit normal, and  $k_L$  completes the right-handed frame.

# 3. Frozen in Time Riccati Equation Based Control

In this work, the Frozen in time Riccati Equation (FTRE)-based control is implemented for the Deputy spacecraft stabilization to a virtual target. The FTRE-based control is the standard infinite-horizon LQR control which is computed by solving the Discrete Algebraic Riccati Equation (DARE),

$$S = Q - A_d^{\mathsf{T}}(t_k) S B_d (R + B_d^{\mathsf{T}}(t_k) S B_d(t_k))^{-1} B_d^{\mathsf{T}}(t_k) S A_d(t_k) + A_d^{\mathsf{T}}(t_k) S A_d(t_k), \tag{5}$$

where  $Q = Q^T \ge 0$  and  $R = R^T > 0$  denote weight matrices for state and control, respectively, and S stands for the solution to DARE at the time instant  $t_k$ , e.g.,  $S = S(t_k)$ . Here  $A_d(t_k)$  and  $B_d(t_k)$  represent the linearized model at the virtual target state (i.e., at  $X_v(t_k)$ ), converted to discrete-time. The resulting control input for the Deputy spacecraft is then given by

$$u_d(t) = K(t_k)(X_d(t_k) - X_v(t_k)), \ \forall t \in [t_k, t_{k+1}), \ k \in \mathbb{Z}_{\geq 0},$$

$$K(t_k) = -(R + B_d^\mathsf{T}(t_k)SB_d(t_k))^{-1}B_d^\mathsf{T}(t_k)SA_d(t_k),$$
(6)

where  $X_{\nu}(t)$  stands for the virtual target for the Deputy spacecraft,  $K(t_k)$  is the control gain, obtained by solving DARE, and  $\{t_k\}_{k=0}^{\infty}$  are discrete time instants. Note that the nominal controller, i.e., FTRE-based controller, is assumed to be able to (at least locally) track  $X_{\nu}(t)$ , which is a time-shifted Chief spacecraft state, for constant time shifts.

## 4. Constraints

During the proximity operation, the Deputy spacecraft must satisfy a variety of constraints. In this study, four types of constraints are considered to demonstrate the effectiveness of the proposed approach. These constraints are imposed on the approach direction, thrust limit, relative velocity when the Deputy spacecraft is near the Chief spacecraft, and exponential stability of the Deputy spacecraft with respect to the time shifted virtual target.

The rendezvous and docking (RVD) mission consists of two main parts: bringing the Deputy spacecraft close to the Chief spacecraft in the rendezvous phase and final approach of the Chief spacecraft in the docking stage. During the RVD mission phase, the Deputy spacecraft has to stay within a prescribed approach direction and satisfy a Line of Sight (LoS) cone angle constraint. The LoS cone angle constraint with LoS half-cone angle  $\alpha$  is given by

$$h_1 = -v(X_c)^{\mathsf{T}} p(X_d - X_c) + \cos(\alpha) ||v(X_c)|| ||p(X_d - X_c)|| \le 0,$$
(7)

where linear maps  $p: \mathbb{R}^n \to \mathbb{R}^{n_{pos}}$  and  $v: \mathbb{R}^n \to \mathbb{R}^{n_{vel}}$  are defined as,

$$p(X) = [[I]_{n_{pos}} [0]_{n_{vel}}]X, \ v(X) = [[0]_{n_{pos}} [I]_{n_{vel}}]X, \tag{8}$$

and where  $n_{pos}$  and  $n_{vel}$  denote the dimension of position and velocity vectors, respectively. Note that  $[I]_i \in \mathbb{R}^i$  and  $[0]_i \in \mathbb{R}^i$  are an identity matrix and null matrix, respectively, with the dimension given by the subscript.

The thrust limit constraint is defined as

$$h_2 = ||u_d|| - u_{\text{max}} \le 0, \tag{9}$$

where  $u_{\text{max}}$  is the maximum magnitude of the control input.

To provide faster response [23], an alternative approach can be used to enforce Eq. (9) using saturation instead of handling Eq. (9) as a constraint via TSG. The saturation limits the magnitude of control input up to the maximum value  $u_{\text{max}}$  while preserving control input direction:

$$u_d(t) := \begin{cases} u_d(t), & \text{if } ||u_d(t)|| \le u_{\text{max}}, \\ u_{\text{max}} \hat{u}_d(t), & \text{if } ||u_d(t)|| > u_{\text{max}}, \end{cases}$$
(10)

where

$$\hat{u}_d(t) = \frac{u_d(t)}{\|u_d(t)\|}. (11)$$

With Eqs. (10)-(11) used to enforce Eq. (9), the TSG accounts for the saturated control input during its prediction stage.

When the Deputy spacecraft gets into close proximity to the Chief spacecraft, the approach velocity constraint is imposed to provide the flexibility to correct misalignment in the docking ports and to reduce the risk of high-speed collisions. Thus, we also define the constraint on the magnitude of the approach velocity that is only activated when the Deputy spacecraft is in the vicinity of the Chief spacecraft, i.e.,

$$||p(X_d - X_c)|| \le \gamma_1, \tag{12}$$

If Eq. (12) holds, the approach velocity is limited by a linearly decreasing function of the relative distance to the Chief,

$$h_3 = \|v(X_d - X_c)\| - \gamma_2 \|p(X_d - X_c)\| - \gamma_3 \le 0, \tag{13}$$

where  $\gamma_1$ ,  $\gamma_2$  and  $\gamma_3$  are predetermined constants set depending on mission requirements.

Until the virtual target matches with the Chief spacecraft, the time shift parameter can be changed every update period by TSG. To ensure that the capability of tracking the virtual target corresponding to the updated time shift parameter is maintained so that the Deputy spacecraft stays within the region of attraction of this virtual target, additional constraints on the predicted trajectory can be added. For instance, one such constraint could be a terminal set constraint which involves the check that the end state of the predicted state trajectory is inside a neighborhood of the virtual target state where this neighborhood is sufficiently small so that it is guaranteed to be in the closed-loop region of attraction. In the subsequent simulations, we impose an additional constraint of the form,

$$h_4 = \eta(X_d(\tau) - X_v(\tau)) - c_1 \|X_d(t_0) - X_v(t_0)\| e^{-\lambda \tau} \le 0, \tag{14}$$

where  $\tau$  in Eq. (14) designates the time since the start of the prediction window and the map  $\eta: \mathbb{R}^n \to \mathbb{R}$  is defined as

$$\eta(X) = \sqrt{p^{\mathsf{T}}(X)p(X) + \gamma_4 \nu^{\mathsf{T}}(X)\nu(X)},\tag{15}$$

 $\gamma_4 > 0$  is a constant used to match position and velocity terms with  $c_1 > 0$ ,  $\lambda > 0$  being positive parameters. Note that the initial virtual target  $X_{\nu}(t_0)$  is determined by a time shift parameter that leads the resulting trajectory to satisfy the first three constraints stated in Eqs. (7), (9), and (13).

#### B. Time Shift Governor

In this work, we use the Time Shift Governor (TSG) to enforce the constraints in spacecraft RVD in an elliptic orbit. The proposed control system is described in Figure 3, where the TSG is augmenting a nominal control system which is made up of spacecraft dynamics and the FTRE-based controller. Instead of directly modifying the nominal controller to enforce constraints, we implement an add-on module, called TSG, to conduct a safe RVD mission with the Chief spacecraft.

To ensure constraint satisfaction, the TSG provides a time-shifted location of the Chief spacecraft as the virtual target to the nominal controller of the Deputy spacecraft. Using the time shift,  $t_{backward}$ , the shifted reference for the Deputy spacecraft controller at time t is determined by,

$$X_{\nu}(t) = X_{C}(t + t_{\text{backward}}). \tag{16}$$

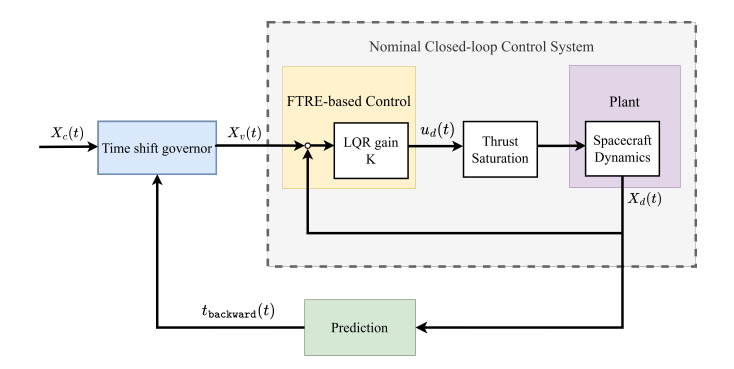


Fig. 3 Diagram of the FTRE-based controller augmented with the TSG to enforce the constraints.

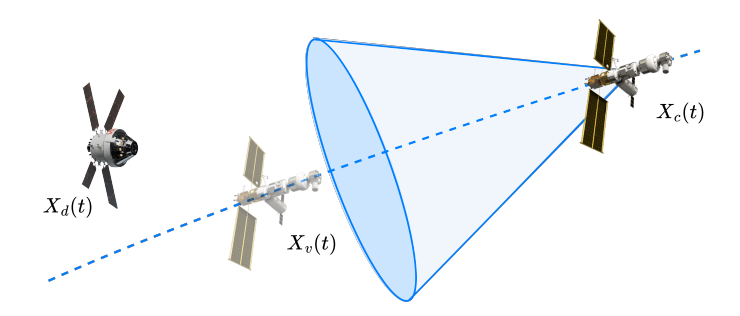


Fig. 4 The Chief, the Deputy, and the virtual target spacecraft in the orbital track.

Assuming the Deputy spacecraft is positioned backward along the orbital track as compared to the Chief spacecraft, we confine the time shift to non-positive values, i.e.,  $t_{backward} \le 0$ . The TSG operates by predicting the closed-loop response of the Deputy spacecraft and the response of Chief spacecraft as it follows the nominal orbit, and checking for constraint violations. If the imposed state and control constraints are satisfied over a sufficiently long prediction horizon, the value of  $t_{backward} \le 0$  is admissible. The TSG then maximizes  $t_{backward}$  subject to the constraint  $t_{backward} \le 0$  and that  $t_{backward}$  is admissible. Over time, this allows the Deputy spacecraft to approach the Chief spacecraft without violating the imposed constraints. Figure 4 illustrates the Chief and Deputy spacecraft and the virtual target.

Similarly to the developments in [16, 17, 20], it can be demonstrated that if 1) a feasible  $t_{backward}$  exists at the initial time instant for the sufficiently long prediction horizon, 2) the nominal controller is stabilizing, and 3) constraints strictly hold in steady-state corresponding to any constant  $t_{backward}$ , then constraints be satisfied by TSG at all future times.

We first initialize the time shift parameter  $t_{\text{backward}}$  to  $t_{\text{backward},-1} \in \mathbb{R}_{<0}$ , such that the predicted trajectory from Eqs. (1), (6) and (16) satisfies all imposed constraints over a sufficiently long prediction horizon. With the initial deviation of the deputy spacecraft with respect to the virtual target, determined by  $t_{\text{backward}}$ , the values of  $c_1, \lambda > 0$  are chosen such that there exists at least one trajectory which avoids any constraint violation.

The TSG updates the time shift parameter  $t_{backward}(t)$  and the set of time shift parameters periodically every  $P_{backward}$  [sec] so that

$$t_{\text{backward}}(t) = t_{\text{backward}}(t_k), \ \forall t \in [t_k, t_k + P_{\text{backward}}). \tag{17}$$

The search interval for the time shift  $t_{\text{backward}}$  parameter at the next time instant  $t_{k+1} = t_k + P_{\text{backward}}$  is restricted to the set

$$t_{\text{backward}}(t_{k+1}) \in \mathcal{T}(t_{k+1}) = \{t_{\text{backward}} \in \mathbb{R}_{\leq 0} | t_{\text{backward}}(t_k) \leq t_{\text{backward}}(t) \leq 0, \ \forall t \geq t_{k+1} \}. \tag{18}$$

# Algorithm 1 Time shift governor algorithm

- 1: Select the initial shift parameter  $t_{\text{backward}} = t_{\text{backward},0} \in \mathbb{R}_{\geq 0}$  at t = 0 such that the resulting trajectory satisfies constraints in Eqs. (7), (9), and (13) using the selected  $t_{\text{backward},0}$  in Eqs. (6) and (16);
- 2: **for**  $k \in \{1, \dots, N_{sim} 1\}$  **do**
- 3:  $\bar{t}_{\text{backward}} = t_{\text{backward}}, \ \underline{t}_{\text{backward}} = 0;$
- 4: **while**  $||\bar{t}_{backward} \underline{t}_{backward}|| > \psi \mathbf{do}$
- 5: Propose a shift parameter:

$$t_{\text{backward,m}} = \frac{\bar{t}_{\text{backward}} + \underline{t}_{\text{backward}}}{2};$$

6: Predict the trajectory with  $t_{backward,m}$  over the time interval  $[t_k, t_k + P_{ref}]$ ,

$$\mathbb{1}_{\text{safe}} = \text{Prediction}(t_k, X_c(t_k), X_d(t_k), X_v(t_k), t_{\text{backward,m}}, [t_k, t_k + P_{\text{ref}}]);$$

7: Update the feasible shift parameter bounds,

$$\begin{cases} \bar{t}_{\text{backward}} = t_{\text{backward,m}}, & \text{if } \mathbb{1}_{\text{safe}} = 1, \\ \underline{t}_{\text{backward}} = t_{\text{backward,m}}, & \text{otherwise;} \end{cases}$$

- 8: end while
- 9: Set  $t_{\text{backward}}(t_k) = \bar{t}_{\text{backward}}$  and  $X_v(t_k) = X_c(t_k + t_{\text{backward}}(t_k));$
- 10: Forward simulate the system over  $[t_k, t_k + P_{backward}]$  using Eqs. (1) and (6);
- 11: **end for**

# **Algorithm 2** Prediction( $X_c(t), X_d(t), t_{lead,m}, t_{pred}$ )

- 1:  $\mathbb{1}_{safe} = 1$ ;
- 2: **for**  $\tau \in \{t, \dots, t + P_{ref}\}$  **do**
- 3: Compute LoS cone angle constraint  $h_1$  in Eq. (7):

$$h_1 = \text{LoS\_cone}(X_d, X_c, \alpha);$$

4: Compute approach velocity constraint  $h_3$  in Eq. (13):

$$\mathbb{1}_{h_3} = \begin{cases} 1, & \text{if } ||p(X_d - X_c)|| \le \gamma_1 \\ 0, & \text{otherwise} \end{cases},$$

$$h_3 = \mathbb{1}_{h_3} \cdot \operatorname{approach\_velocity}(X_d, X_c, \gamma_2, \gamma_3);$$

5: Compute exponential stability constraint  $h_4$  in Eq. (14):

$$h_4$$
 = exponential\_stability( $t, X_d, X_v, c(X_d(t_0), X_v(t_0)), \lambda$ );

- 6: If  $\max_{j \in \{1,3,4\}} \{h_j\} \ge 0$ , then  $\mathbb{1}_{safe} = 0$  and **break**;
- 7: end for
- 8: return  $\mathbb{1}_{safe}$ .

Table 1 Classical orbital elements of the reference Molniya orbit

SMA, a	Eccentricity, e	Inclination, i	RAAN, Ω	Argp, ω	True anomaly, $\nu$
26646.6808 [km]	0.74	62.8 [deg]	0 [deg]	280 [deg]	0 [deg]

We use one period of the osculating orbit, denoted by  $P_{ref}$ , as the prediction horizon. Using Eqs. (2), (6), and (10), the feasibility (admissibility) of the updated time shift parameter is determined by checking for the absence of constraint violations by the predicted trajectory of the closed-loop model over a sufficiently dense time grid over the prediction horizon, i.e., for  $t \in [t, t + P_{ref}]$ .

Approximations can be employed to reduce the online computational effort. For instance, in evaluating the admissibility of a particular value of  $t_{\text{backward}}(t_{k+1})$  at the time instant  $t_{k+1}$ , we need FTRE control gains K which depend on Deputy spacecraft model linearization at states  $X_c(t_{k+1} + t_{\text{backward}}(t_{k+1}) + kP_{\text{backward}})$ ,  $k \in \mathbb{Z}_{\geq 0}$ . These time instants change as  $t_{\text{backward}}(t_{k+1})$  is varied inside  $\mathcal{T}(t_{k+1})$  during optimization. To reduce the number of DAREs that need to be solved, we can simply pre-compute a few of FTRE control gains along the predicted Chief spacecraft orbit over the time interval  $[t_k + t_{\text{backward}}(t_k), t_k + P_{\text{ref}}]$  and employ elementwise interpolation of the pre-computed gain values. This strategy has been employed in the subsequent simulation results.

#### IV. Simulation Results

In this section, we report simulation results of the Deputy spacecraft rendezvous and docking (RVD) to the Chief spacecraft on a Molniya orbit.

## A. Simulation specifications

In this simulation, we consider the Chief spacecraft following the reference Molniya orbit [3]. See Fig. 5 for a plot of the nominal Molniya orbit, which has a period of 721.5 minutes, corresponding to the orbital elements stated in Table. 1. The one osculating orbital period  $P_{\text{ref}}$  is chosen as the prediction horizon for the TSG at a time instant t, i.e., the prediction is performed over the time interval,  $[t, t + P_{\text{ref}}]$ . The gravitational parameter is  $\mu = 398600.4418 \text{km}^2/\text{sec}^3$ . The zonal gravitational harmonics constant and equatorial radius of the primary body in Eq. (4) are  $J_2 = -C_{2,0} = 4.8417 \times 10^{-4}$  and  $r_{eq} = 6378.1363 \text{km}$ .

The nominal controller of the Deputy spacecraft is the FTRE-based controller in Eq. (6) with an LQR gain  $K(t_k)$  computed for the following state and control weighting matrices, Q and R:

$$Q = diag(10, 10, 10, 1, 1, 1), \quad R = diag(1, 1, 1). \tag{19}$$

The LQR gain  $K(t_k)$  is computed from a linearized model at the virtual target, corresponding to  $t_{\text{backward}}$ . We consider constraints defined with the following values: 20 [deg] of the Half-cone angle  $\alpha$  in Eq. (7), 50 [cm<sup>2</sup>/sec<sup>2</sup>] of the maximum thrust in Eq. (9),  $\gamma_1 = 5$  [km],  $\gamma_2 = 20$  [rad/s],  $\gamma_3 = 10^{-3}$  [km/s] of the approach velocity constraint in Eq. (12), (13), and  $c_1 = 2$  [km],  $\lambda = 1.5 \times 10^{-5}$  [rad/sec],  $\gamma_4 = 1$  [sec<sup>2</sup>] in the stability constraint in Eq. (14).

# **B.** Results

Table. 2 states the initial condition for the Deputy spacecraft expressed in the ECI frame. The Deputy spacecraft initially departs to the Chief spacecraft from about 4874 km backward in the orbital track. See Fig. 6 for a plot of the Chief (cross) and the Deputy (circle) with the TSG for the constrained RVD mission on a Molniya orbit. After 609 minutes,  $t_{end}$ , of simulation, the Deputy spacecraft closes within meters, e.g.,  $||p(X_d(t_{end}) - X_c(t_{end}))|| < 1 \text{ m}$ .

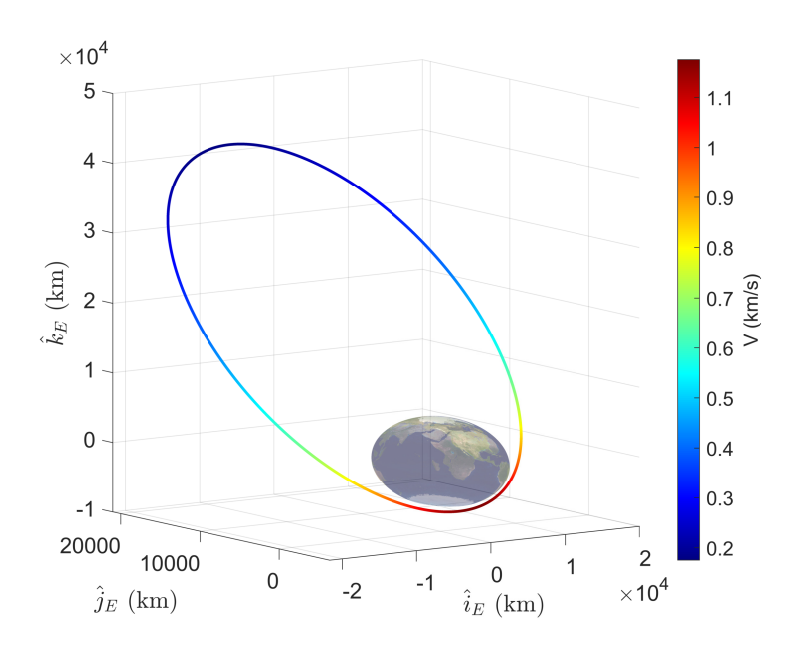


Fig. 5 Reference trajectory for Chief spacecraft on a Molniya orbit.

Table 2 Initial condition for the Deputy spacecraft to the Chief spacecraft, e.g.,  $X_d(0) - X_c(0)$ 

$\delta x_0$	$\delta y_0$	$\delta z_0$	$\delta \dot{x}_0$	$\delta \dot{y}_0$	$\delta \dot{z}_0$
-4872.6495 [km]	54.8262 [km]	106.6803 [km]	-0.6190 [km/s]	-1.7186 [km/s]	-3.3441 [km/s]

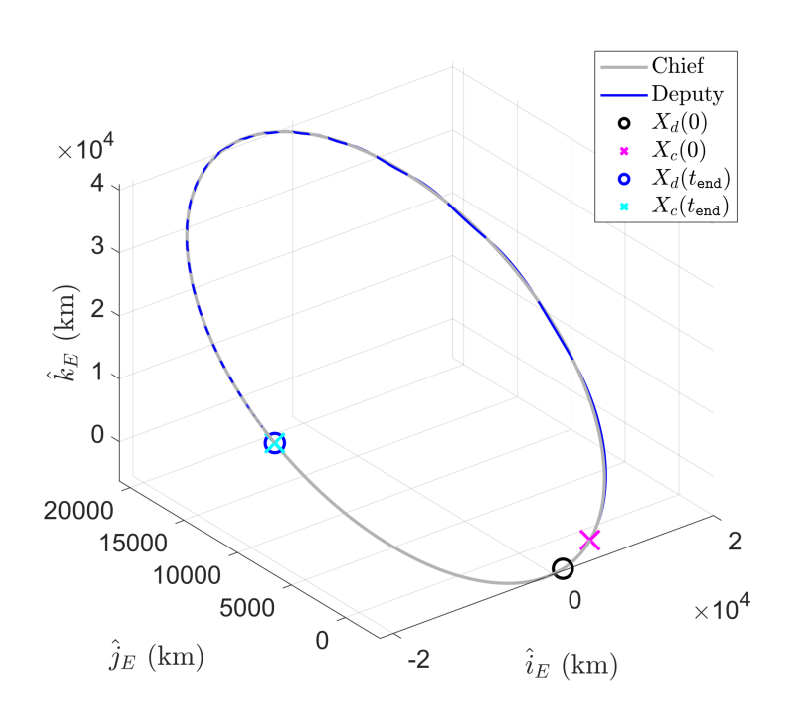
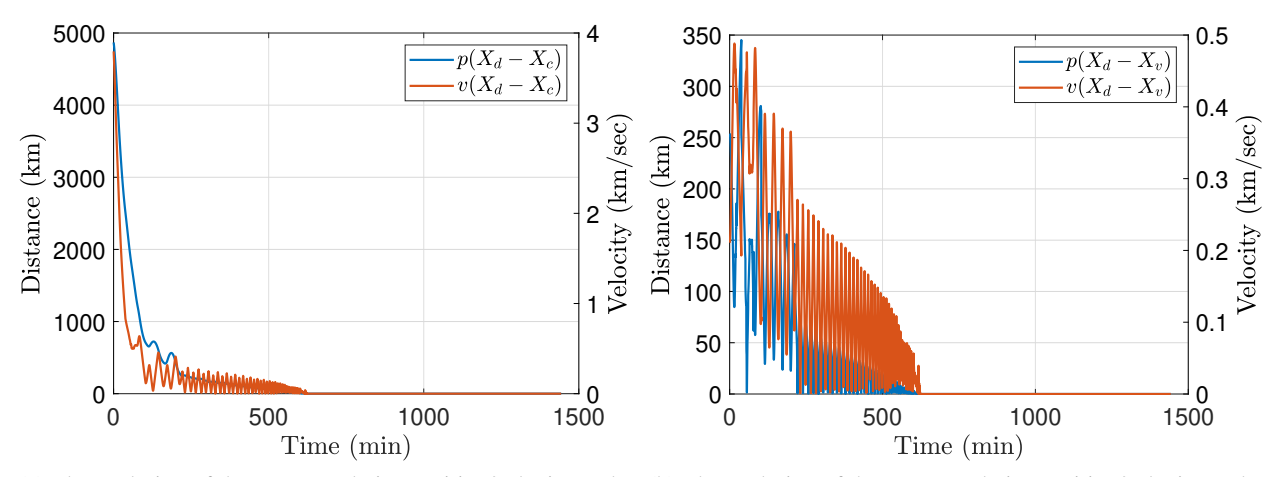


Fig. 6 Spacecraft rendezvous trajectories with initial and first achieved points at time  $t_{\rm end} \simeq 609$  minutes:  $X_c(0)$  (magenta),  $X_d(0)$  (black),  $X_c(t_{\rm end})$  (cyan),  $X_d(t_{\rm end})$  (blue).

Figures 7a and 7b show the Deputy spacecraft position (blue) and velocity (orange) relative to the Chief spacecraft and to the virtual target in the ECI frame. The Deputy spacecraft becomes gradually closer to the Chief spacecraft and successfully achieves the RVD mission. Figure. 7 illustrates how the TSG governs the RVD mission by shifting the virtual target of the Deputy in the VNB frame. With the TSG handling the virtual target, the proposed control strategy demonstrates its capability to complete the RVD mission without constraint violation.



(a) The evolution of the Deputy relative position/velocity to the (b) The evolution of the Deputy relative position/velocity to the Chief spacecraft during the RVD using the TSG.

virtual target spacecraft during the RVD using the TSG.

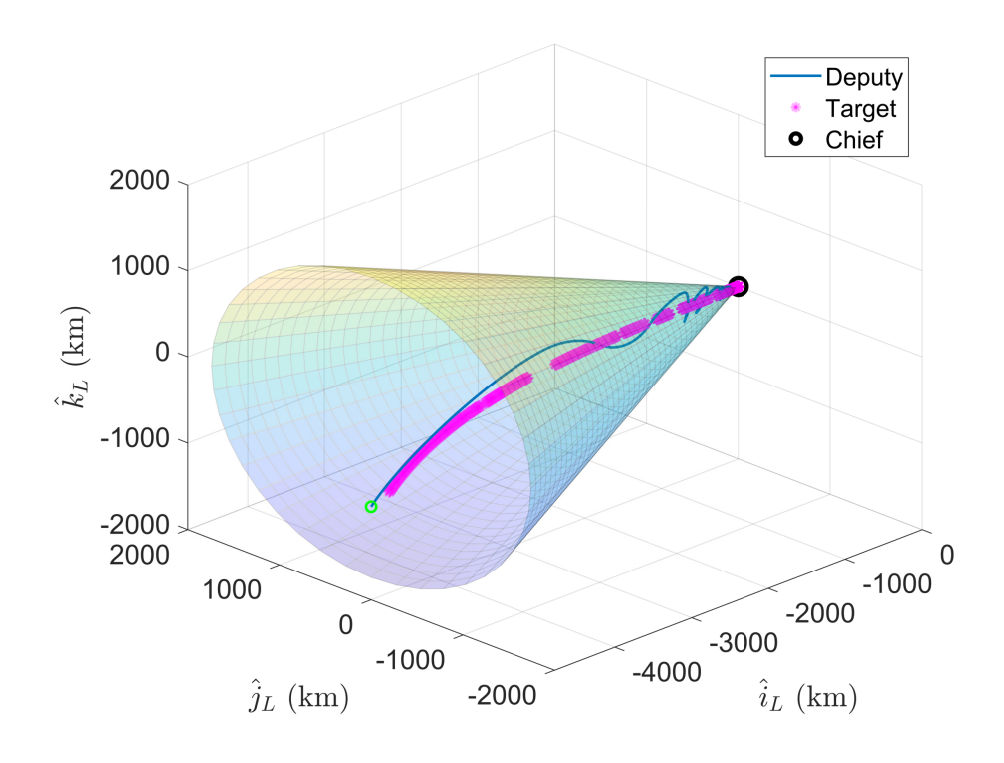


Fig. 7 The Deputy spacecraft (blue line) and the virtual target (magenta asterisk) trajectories in the local VNB frame, as defined in Section III.A.2.

Figures 8a,8b, 8c, and 8d show the performance of our proposed control approach with the TSG during the RVD mission. Figure 8a indicates the Line of Sight (LoS) cone angle constraint  $h_1$  is effectively handled by the TSG. In Fig. 8b, the thrust constraint  $h_2$  is presented. Note that the saturation in Eq. (10) addresses this constraint. Figure 8c shows the time history of the relative velocity constraint  $h_3$ . The TSG is capable of enforcing this constraint when the Deputy spacecraft close within 5km. In other words, during the docking stage, the approach velocity is successfully handled by the TSG in the proximity of the Chief spacecraft. The exponential convergence constraint is presented as a function of time in Fig. 8d. Since the radius of the closed ball is shrinking exponentially, this constraint ensures that the nominal closed-loop system of the Deputy spacecraft converges to the virtual target. Moreover, the virtual target reaches the Chief spacecraft, ensuring that the Deputy spacecraft also converges the Chief spacecraft.

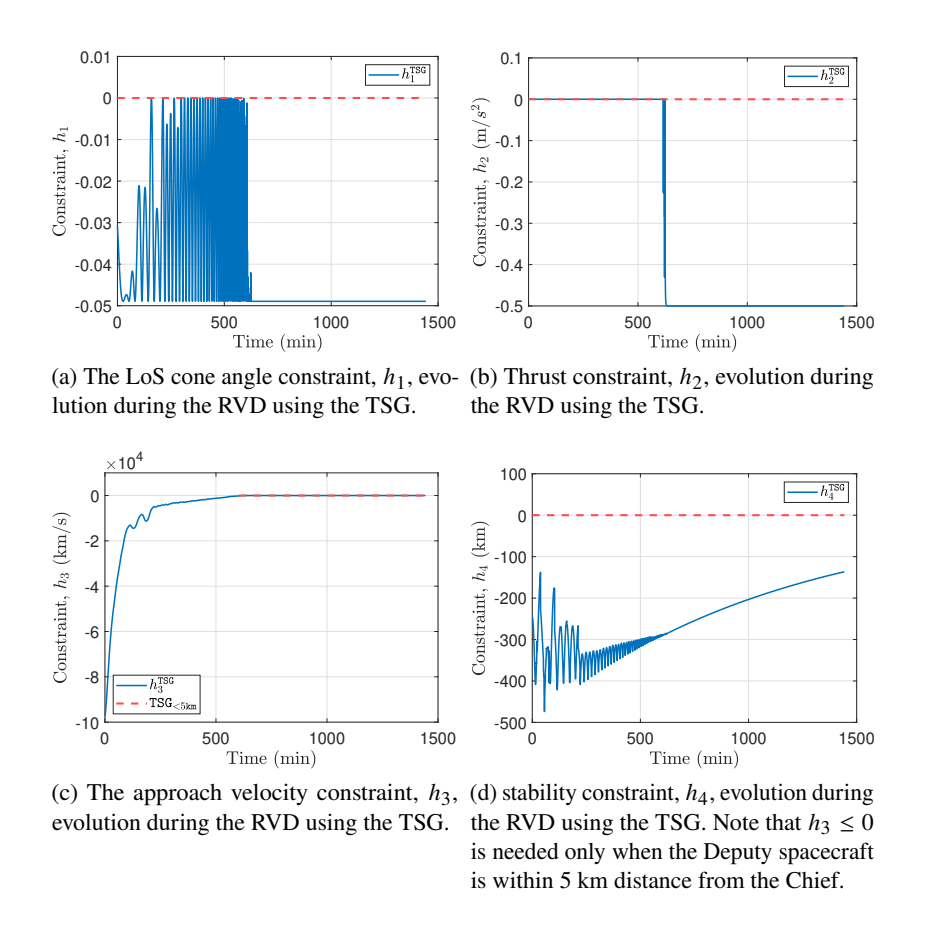


Figure 8 indicates how the time shift parameter is adjusted as a function of time. The time shift parameter,  $t_{\text{backward}}$ , begins with the initial admissible value,  $t_{\text{backward},0}$ , and changes to the largest admissible value by the TSG at every update. The time shift value continues increasing until it achieves a sufficiently large value for which the Deputy spacecraft can approach the Chief spacecraft. After the time shift parameter is equal to zero, the Deputy spacecraft is able to achieve the Chief spacecraft solely by the nominal controller without constraint violations.

## V. Conclusion

In this paper, we developed the time shift governor (TSG) for the spacecraft rendezvous and docking (RVD) missions in elliptic Earth orbits. The TSG has been demonstrated to be able to enforce various constraints during the proximity operation, such as on the approach direction, relative velocity, thrust limit,

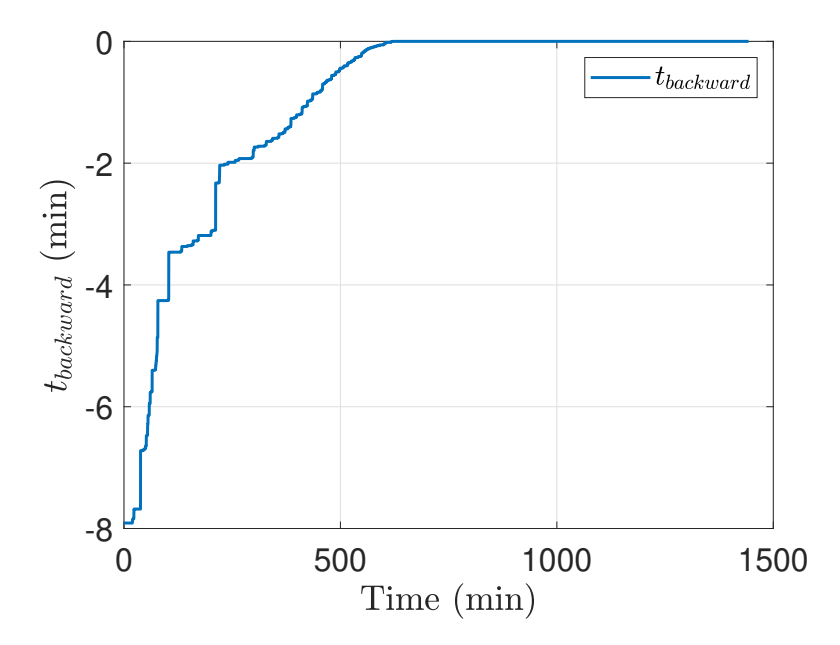


Fig. 8 The evolution of the time shift parameter during the rendezvous in minutes.

and exponential convergence to the target. To enforce the constraints, a virtual target, selected as a time-shifted Chief spacecraft trajectory, is provided by TSG to the nominal controller of the Deputy spacecraft. The simulated RVD in the elliptic Earth orbit shows the effectiveness of the TSG in enforcing constraints.

# VI. Acknowledgments

This research is supported in part by the National Science Foundation Award CMMI-1904394. The authors would like to thank Mr. Kaiwen Liu for the past collaboration on the related TSG methodology for spacecraft automated rendezvous in Halo orbits [18] in a three body problem setting; insights from that work have been instrumental to designing TSG for elliptic orbits.

#### References

- [1] Foust, J., "Sierra Nevada Hopes Dream Chaser Finds "Sweet Spot" of ISS Cargo Competition," Space News, 2015.
- [2] Clark, S., "Launch Schedule," Spaceflight Now, 2023.
- [3] Kolyuka, Y. F., Ivanov, N., Afanasieva, T., and Gridchina, T., "Examination of the lifetime, evolution and re-entry features for the "Molniya" type orbits," *Proceedings of the 21st International Symposium on Space Flight Dynamics—21st ISSFD, Toulouse, France*, Vol. 650, 2009, pp. 30–110.
- [4] Evans, B., "Sirius Rising: Proton-M Ready to Launch Digital Radio Satellite Into Orbit," America Space, 2013.
- [5] Jenkin, A. B., McVey, J. P., Wilson, J. R., and Sorge, M. E., "Tundra disposal orbit study," *Proceedings of the 7th European Conference on Space Debris, Darmstadt*, 2017.
- [6] Jewison, C. M., "Guidance and control for multi-stage rendezvous and docking operations in the presence of uncertainty," Ph.D. thesis, Massachusetts Institute of Technology, 2017.
- [7] Dong, H., and Akella, M. R., "Autonomous rendezvous and docking of spacecraft under 6-DOF motion constraints," 2017 IEEE 56th Annual Conference on Decision and Control (CDC), IEEE, 2017, pp. 4527–4532.
- [8] Lopez, I., and McInnes, C. R., "Autonomous rendezvous using artificial potential function guidance," *Journal of Guidance, Control, and Dynamics*, Vol. 18, No. 2, 1995, pp. 237–241.

- [9] Roger, A. B., and McInnes, C. R., "Safety constrained free-flyer path planning at the international space station," *Journal of Guidance, Control, and Dynamics*, Vol. 23, No. 6, 2000, pp. 971–979.
- [10] Weiss, A., Baldwin, M., Erwin, R. S., and Kolmanovsky, I., "Model predictive control for spacecraft rendezvous and docking: Strategies for handling constraints and case studies," *IEEE Transactions on Control Systems Technology*, Vol. 23, No. 4, 2015, pp. 1638–1647.
- [11] Park, H., Di Cairano, S., and Kolmanovsky, I., "Model predictive control for spacecraft rendezvous and docking with a rotating/tumbling platform and for debris avoidance," *Proceedings of the 2011 American control conference*, IEEE, 2011, pp. 1922–1927.
- [12] Bodin, P., Larsson, R., Nilsson, F., Chasset, C., Noteborn, R., and Nylund, M., "PRISMA: An in-orbit test bed for guidance, navigation, and control experiments," *Journal of Spacecraft and Rockets*, Vol. 46, No. 3, 2009, pp. 615–623.
- [13] Larsson, R., Berge, S., Bodin, P., and Jönsson, U., "Fuel efficient relative orbit control strategies for formation flying and rendezvous within PRISMA," *Advances in the Astronautical Sciences*, Vol. 125, 2006, pp. 25–40.
- [14] Richards, A., and How, J. P., "Robust variable horizon model predictive control for vehicle maneuvering," *International Journal of Robust and Nonlinear Control: IFAC-Affiliated Journal*, Vol. 16, No. 7, 2006, pp. 333–351.
- [15] Vazquez, R., Gavilan, F., and Camacho, E. F., "Pulse-width predictive control for LTV systems with application to spacecraft rendezvous," *Control Engineering Practice*, Vol. 60, 2017, pp. 199–210.
- [16] Frey, G. R., Petersen, C. D., Leve, F. A., Garone, E., Kolmanovsky, I. V., and Girard, A. R., "Time shift governor for coordinated control of two spacecraft formations," *IFAC-PapersOnLine*, Vol. 49, No. 18, 2016, pp. 296–301.
- [17] Frey, G. R., Petersen, C. D., Leve, F. A., Garone, E., Kolmanovsky, I. V., and Girard, A. R., "Parameter governors for coordinated control of n-spacecraft formations," *Journal of Guidance, Control, and Dynamics*, Vol. 40, No. 11, 2017, pp. 3020–3025.
- [18] Kim, T., Liu, K., Kolmanovsky, I. V., and Girard, A. R., "Time shift governor for constraint satisfaction during low-thrust spacecraft rendezvous in near rectilinear halo orbits," 2023 IEEE conference on control technology and applications (CCTA), IEEE, 2023.
- [19] Cichella, V., Kaminer, I., Dobrokhodov, V., Xargay, E., Choe, R., Hovakimyan, N., Aguiar, A. P., and Pascoal, A. M., "Cooperative path following of multiple multirotors over time-varying networks," *IEEE Transactions on Automation Science and Engineering*, Vol. 12, No. 3, 2015, pp. 945–957.
- [20] Kolmanovsky, I. V., and Sun, J., "Parameter governors for discrete-time nonlinear systems with pointwise-in-time state and control constraints," *Automatica*, Vol. 42, No. 5, 2006, pp. 841–848.
- [21] Hilton, W., "An Introduction to the Mathematics and Methods of Astrodynamics RH Battin. American Institute of Aeronautics and Astronautics, Washington, DC. 1987. 796 pp. Illustrated. 49.95 (Non-Members)." *The Aeronautical Journal*, Vol. 93, No. 923, 1989, pp. 111–111.
- [22] Bate, R. R., Mueller, D. D., White, J. E., and Saylor, W. W., *Fundamentals of astrodynamics*, Courier Dover Publications, 2020.
- [23] Cotorruelo, A., Limon, D., and Garone, E., "Output admissible sets and reference governors: Saturations are not constraints!" *IEEE Transactions on Automatic Control*, Vol. 65, No. 3, 2019, pp. 1192–1196.